Research Square

Preprints are preliminary reports that have not undergone peer review.
They should not be considered conclusive, used to inform clinical practice,
or referenced by the media as validated information.

# In silico design and physicochemical characterisation of a dual-action intranasal nanoparticle formulation for Alzheimer's disease

**Rahul Rao**
Iroquois Ridge High School
**Vivaan Kar**
Iroquois Ridge High School
**Brian Webb**
b.webb@mail.utoronto.ca

University of Toronto

**Article**

**Keywords:** Alzheimer's disease, intranasal drug delivery, 7,8-dihydroxyflavone, EF24, Brain derived neurotrophic factor (BDNF) - Tropomyosin receptor kinase B (TrkB) signalling, Tau protein

**Posted Date:** September 28th, 2026

**DOI:** https://doi.org/10.21203/rs.3.rs-10822803/v1

**License:** This work is licensed under a Creative Commons Attribution 4.0 International License.
Read Full License

**Additional Declarations:** No competing interests reported.

# Abstract

Approved Alzheimer's disease therapies fail to address the two drivers of cognitive decline: loss of BDNF-TrkB signalling and accumulation of hyperphosphorylated tau protein. We designed and evaluated an intranasal poly(lactic-co-glycolic acid) (PLGA) nanoparticle co-loading two small molecules − 7,8-Dihydroxyflavone, a TrkB agonist, and EF24, a curcumin analog that binds to tau. The design was evaluated across molecular docking, molecular dynamics, ADMET prediction, pharmacokinetic simulation, and nanoparticle synthesis and characterisation. Among four compounds tested, 7,8-Dihydroxyflavone showed the strongest predicted TrkB binding (ΔG = -9.079 kcal $mol^{-1}$), exceeding donepezil and memantine, while EF24 showed the strongest predicted tau binding (-5.068 kcal $mol^{-1}$) and comparable GSK-3β affinity to other compounds. Over 20 ns molecular dynamics simulations, both candidates remained stably bound to their targets (ligand RMSD ≤ 3.1 Å), whereas both approved drugs dissociated. Both compounds were predicted to be blood-brain-barrier permeant and drug-like, with predicted median lethal doses exceeding those of the approved comparators. Intranasal delivery increased predicted brain exposure over oral administration across all pharmacokinetic metrics. Nanoparticles synthesised across three batches were consistent in size, dispersity and surface charge, falling within published specifications for intranasal delivery (152 nm; polydispersity 0.21; zeta potential − 26 mV). These findings identify this approach as a mechanistically grounded candidate warranting further in-vitro and in-vivo validation.


# Introduction

Currently, Alzheimer's disease (AD) affects over 55 million people worldwide, a number expected to exceed 139 million by 2050 [1]. According to the World Health Organization, AD is the most common cause of dementia and the seventh leading cause of death worldwide [2]. Current approved treatments for AD do not change the overall trajectory of the disease [3]. Cholinesterase inhibitors (donepezil, rivastigmine, and galantamine) raise acetylcholine transiently and offer modest, temporary cognitive improvements that last roughly a year [3, 4]; memantine regulates excitotoxic calcium entry within NMDA receptors, with similar limited effect[4]. Anti-amyloid antibodies (lecanemab and donanemab) slow decline in early stages of AD but require intravenous infusion, repeated MRI surveillance for amyloid-relating imaging abnormalities (ARIA), and careful patient selection [5–7]. No current treatments act on the two key mechanisms driving neurodegeneration in AD: the loss of BDNF-TrkB signalling and the aggregation of toxic tau protein [8]. BDNF supports neurons and synapses by binding TrkB and activating the PI3K-Akt, MAPK/ERK and PLC-γ pathways. In AD, this signalling is weakened in various ways. Amyloid-β disrupts calcium signalling in neurons, blocking the transcription factor CREB and shutting down BDNF production [10]. Tau tangles disrupt microtubules, blocking the transport of BDNF to synapses [11]. Amyloid also triggers epigenetic changes that silence the BDNF gene [10]. As BDNF signalling declines, synapses weaken and neurons become more vulnerable to damage [12, 13]. Tau breaks down through a similar process. The same calcium disruption that suppresses BDNF activates kinases that

hyperphosphorylate tau (GSK-3β, CaMKII and CDK5), causing it to detach from microtubules and aggregate into clumps [11]. This impairs neuronal transport and allows tau to spread between cells.

Additionally, the delivery of therapeutics to the brain is impeded by the blood brain barrier, blocking roughly 98% of small molecules administered systemically [14]. However, nasal administration bypasses this barrier, carrying the drug along the olfactory and trigeminal nerves directly into the central nervous system. Furthermore, encapsulation within PLGA nanoparticles protects against nasal enzymes and allows for both tunable uptake and controlled release within the brain [15].

Two molecules are plausible candidates for both criteria - with suitability for intranasal delivery and reported activity at AD protein targets. 7,8-Dihydroxyflavone is a synthetic flavone that acts as a TrkB agonist, reproducing much of BDNF's downstream signalling in cell and animal models [16, 17]. EF24, a curcumin analogue with superior bioavailability than curcumin [18], has been proposed to interfere with tau aggregation and GSK-3β activity, though less established in literature than 7,8-Dihydroxyflavone.

Here we present a systematic, multi-stage evaluation of a dual-action intranasal PLGA nanoparticle co-loading 7,8-Dihydroxyflavone and EF24. Both candidates and two approved therapeutics were docked against TrkB, tau and GSK-3β; 20 ns molecular dynamics simulations were run on all twelve complexes; ADMET properties were predicted; pharmacokinetics of oral and intranasal delivery were simulated; and the co-loaded particle was synthesized and characterised. Across these five in-silico and in-vitro experiments, 7,8-Dihydroxyflavone and EF24 were predicted to engage their targets more strongly than the approved comparators and to carry a more favourable predicted toxicity profile, intranasal delivery was predicted to increase brain exposure substantially, and the formulation fell within published specifications for nanoparticle size, uniformity and surface charge.

# Results

### 7,8-Dihydroxyflavone and EF24 bind to their intended targets more strongly than approved drugs

7,8-Dihydroxyflavone, EF24, donepezil and memantine were docked against TrkB, tau, and GSK-3β in SwissDock using the AutoDock Vina scoring function, with three docking runs per pair [19,20]. Mean binding free energies are given in Fig. 1 and Table 1.

**Table 1. Molecular docking ΔG values (kcal mol⁻¹) for all compound–protein pairs.**

| Compound | TrkB receptor ΔG | Tau protein ΔG | GSK-3β ΔG |
|---|---|---|---|
| 7,8-Dihydroxyflavone | −9.079 | −4.681 | −7.345 |
| EF24 | −7.920 | −5.068 | −7.796 |
| Donepezil | −7.796 | −4.617 | −7.794 |
| Memantine | −6.036 | −3.519 | −6.914 |

ΔG, predicted free energy of binding; more negative values indicate stronger predicted affinity. Values are the mean of three docking runs per pair. Differences below ~1 kcal mol⁻¹ are within the scoring function's uncertainty.

7,8-Dihydroxyflavone showed the strongest predicted binding to TrkB of the four compounds, at -9.079 kcal mol⁻¹, 1.3 kcal mol⁻¹ ahead of donepezil and 3.0 kcal mol⁻¹ ahead of memantine, a margin that exceeds the approximately 1 kcal mol⁻¹ uncertainty of this scoring method. EF24 showed the strongest predicted tau binding of the four compounds (−5.068 kcal mol⁻¹). At GSK-3β, EF24, donepezil and 7,8-Dihydroxyflavone fell within 0.5 kcal mol⁻¹ of one another, a margin below the scoring function's resolution; these three should be considered comparable rather than differentiable at this target. Memantine was the weakest binder across all three targets, which is consistent with its NMDA receptor pharmacology. Docking evaluates a single static pose, and therefore, subsequent to the completion of molecular docking experiments, dynamics simulations were conducted.

**Both candidate compounds remain stably bound in molecular dynamics simulations whereas approved drugs dissociate**

20 ns of molecular dynamics were run on all twelve protein–ligand complexes in GROMACS, prepared in CHARMM-GUI with the CHARMM36m force field, TIP3P water and 0.15 M KCl. Stability was quantified by ligand RMSD, protein backbone RMSD and mean hydrogen-bond count (Fig. 2; full per-complex values for all twelve pairs are provided in Table S1).

The folded targets remained structurally intact throughout the simulations, with TrkB and GSK-3β backbone RMSD stabilizing within 2.0–2.4 Å. Tau's higher backbone RMSD (3.0-3.8 Å) reflects its intrinsically disordered nature rather than trajectory instability, consistent with the absence of a defined native fold for this protein (Fig. 2a). 7,8-Dihydroxyflavone remained stably bound within the TrkB pocket throughout the trajectory (ligand RMSD 2.2 Å) and exhibited the highest mean hydrogen-bond count of all complexes examined (3.2), with a well-anchored binding pose (Fig. 2b,c). EF24 also maintained stable engagement at both of its targets, tau (RMSD 2.6 Å) and GSK-3β (RMSD 3.1 Å), remaining within the respective binding pockets for the duration of the simulation. The FDA-approved comparators did not sustain stable complexes: donepezil sat at the 3.8 Å threshold of trajectory stability at TrkB and dissociated from tau (4.6 Å) and GSK-3β (4.8 Å), while memantine dissociated from all three targets (RMSD range 4.2–5.8 Å). Notably, donepezil's docking score was competitive with that of investigational compounds. Its trajectory was not stable - underscoring that a favorable static pose is not sufficient evidence of a stable complex, and that temporal stability can only be resolved through molecular dynamics. As these represent three 20-ns trajectories per complex, they are best interpreted as distinguishing stable from unstable binding modes rather than resolving fine-grained affinity differences among the stable complexes.

**Predicted ADMET profiles favour the candidate compounds**

SwissADME and admetSAR 2.0 predicted all four compounds to be blood brain barrier permeant and have high drug-likeness scores (Table 2; full predicted physicochemical and toxicity profiles are given in Table S2) [21,22].

**Table 2. Predicted ADME and toxicity summary for all tested compounds.**

| Compound | LogP | LD50 (mg $kg^{-1}$) | Ames | Key notes |
|---|---|---|---|---|
| 7,8-Dihydroxyflavone | 2.35 | 2,200 | Negative | BBB-permeant; drug-like; predicted oral cardiac/hepatic signals reduced by nanoparticle encapsulation |
| EF24 | 3.87 | 2,000 | Positive (mild) | BBB-permeant; drug-like; predicted ocular irritation less relevant in encapsulated form |
| Donepezil | 4.00 | 45 | Positive | High lipophilicity; lowest predicted LD50 of the four |
| Memantine | 2.85 | 370 | Negative | Skin, lung and ocular toxicity predicted at repeated doses |

LogP, consensus lipophilicity (SwissADME); LD50, predicted rat oral median lethal dose (admetSAR 2.0). All values are computational predictions, not measured data.

7,8-Dihydroxyflavone was predicted to have appropriate lipophilicity for the CNS (LogP 2.35) and returned a negative Ames prediction. EF24 was predicted to be more lipophilic (LogP 3.87) and returned a weakly positive Ames prediction. These are predicted rather than measured values, no experimental toxicology was performed, and whether encapsulation alters them was not tested in this study. Acute-toxicity predictions for candidates differed drastically from donepezil, whose predicted rat oral LD50 (45 mg $kg^{-1}$) was 44- to 49-fold lower than those of 7,8-Dihydroxyflavone (2,200 mg $kg^{-1}$) and EF24 (2,000 mg $kg^{-1}$).

**Intranasal delivery increases predicted brain exposure**

Oral and intranasal delivery simulations were conducted of both compounds in PK-Sim across a 100-individual virtual adult population parameterised to Canadian demographics, at a 50 mg dose over 24 h (Fig. 3, Table 3).

**Table 3. Simulated pharmacokinetics for oral versus intranasal delivery of 7,8-Dihydroxyflavone and EF24.**

| Compound and route | Cmax (μmol $L^{-1}$) | Tmax (h) | AUC (μmol·min $L^{-1}$) |
|---|---|---|---|
| 7,8-Dihydroxyflavone — Oral | 0.18 | 2.75 | 182.04 |
| 7,8-Dihydroxyflavone — Intranasal | 115.63 | 0.05 | 28,288.58 |
| EF24 — Oral | 0.00765 | 2.75 | 6.74 |
| EF24 — Intranasal | 8.53 | 0.05 | 662.12 |

Cmax, peak brain concentration; Tmax, time to peak; AUC, 24-hour brain area under the curve. Means of three simulation runs. Absolute magnitudes depend on estimated parameters; the intranasal-over-oral direction is the reliable result.

Intranasal delivery increased brain exposure for both compounds across every metric. Peak brain concentration and 24-h brain AUC rose substantially, and predicted time to peak fell from 2.75 h to 0.05 h. In the model, the increases spanned two to three orders of magnitude - Cmax rose 642-fold for 7,8-Dihydroxyflavone and 1115-fold for EF24. Because predicted improvements were based on absorption and plasma protein binding values from published literature rather than direct measurements for these compounds, exact numerical values were treated with caution. Rather, the key identified finding was the consistent advantage of intranasal delivery as opposed to oral, which was observed for both compounds across all three evaluation metrics. This outcome is biologically plausible because intranasal administration allows drugs to reach the brain through the olfactory pathway, bypassing both hepatic first-pass metabolism and the blood–brain barrier, thereby improving brain delivery.

**The co-loaded nanoparticle is reproducible and meets olfactory-delivery specifications**

Three independent batches of PLGA nanoparticles co-loading 7,8-Dihydroxyflavone and EF24, prepared by oil-in-water emulsion with solvent evaporation, were characterised by dynamic and electrophoretic light scattering on a Malvern Zetasizer Nano ZS (Table 4, Fig. 4; optical micrograph of synthesised nanoparticle is provided in Figure S1).

**Table 4. Physical characterisation of PLGA nanoparticle batches co-loading 7,8-Dihydroxyflavone and EF24.**

| Batch | Z-average diameter (nm) | PDI | Zeta potential (mV) |
|---|---|---|---|
| 1 | 154 | 0.21 | −26 |
| 2 | 148 | 0.19 | −25 |
| 3 | 155 | 0.21 | −27 |
| Mean ± SD | 152 ± 4 | 0.21 ± 0.02 | −26 ± 1 |

PDI, polydispersity index (cumulant fit). Zeta potential measured in isotonic saline pH 6.5. Mean ± SD across n = 3 independently prepared batches.

All three batches fell within published specifications for intranasal olfactory delivery and were closely comparable. They had a mean diameter 152 ± 4 nm, within the 100–200 nm window for olfactory-neuron uptake without rapid clearance[15]; polydispersity 0.21 ± 0.02, below the 0.3 monodispersity threshold; and zeta potential −26 ± 1 mV, beyond the ±20 mV colloidal-stability threshold. Such consistency is consistent with a reproducible preparation, although reproducibility beyond three batches, one operator and one instrument was not assessed.

# Discussion

To our knowledge, this is the first report of a paper combining EF24 and 7,8-Dihydroxyflavone in a single PLGA nanoparticle. The combination is directed at two mechanisms implicated in AD progression, the loss of BDNF-TrkB signalling and the aggregation of tau, rather than at the cholinergic and glutamatergic symptoms addressed by current therapy. Across the five analyses reported here, both compounds were predicted to bind their intended targets more strongly than donepezil and memantine, held those poses in simulation where the approved comparators did not, returned favourable predicted ADMET profiles, and were formulated into a nanoparticle preparation consistent across three independent batches. The result is a mechanistically coherent and physically preparable candidate.

The strongest and most mechanistically interpretable result is 7,8-Dihydroxyflavone's binding affinity to TrkB. Its docking preference, dynamic stability and dense hydrogen-bond network together describe a well-anchored agonist interaction. Such an interaction would be a prerequisite for sustaining the PI3K–Akt and MAPK/ERK signalling that BDNF drives, although no signalling was measured in this study [9, 16]. EF24's predicted engagement of tau and GSK-3β is consistent with an anti-tau mechanism. EF24 acts on both the aggregation interface and the kinase that hyperphosphorylates tau. However, we interpret these results more conservatively than TrkB. Tau is intrinsically disordered, therefore docking and short simulations model it imperfectly, and EF24's anti-tau activity is less established in the literature than 7,8-Dihydroxyflavone's TrkB agonism [18]. It is therefore in need of direct experimental confirmation.

The difference between docking and dynamics for the approved drugs is important to consider. Donepezil achieved a strong TrkB docking score yet failed to hold its pose over 20 ns, demonstrating how a combination of static and dynamic docking helps determine a stable interaction [23]. Combining the two methods and considering only complexes that performed well in both provided a more reliable filter and supported the strength of 7,8-Dihydroxyflavone–TrkB and EF24–tau/GSK-3β interactions.

The pharmacokinetic simulations consistently favoured intranasal over oral delivery for peak brain concentration. This is in agreement with the established advantage of olfactory transport for CNS-active compounds in literature [15]. The absolute changes in concentration through delivery methods are large and are best read as estimates, since they depend on absorption and protein-binding parameters

established from the literature rather than measured for these compounds. However, the reliable conclusion is the consistent direction and effect, seen across both compounds and all three metrics.

The nanoparticle results indicate that the two-drug particle can be prepared to specification and was reproducible across three independent batches. Encapsulation efficiency, drug loading and release kinetics were not measured in-vitro and are future experimental priorities.

This work prepared nanoparticles loaded with 7,8-dihydroxyflavone and EF24 and used in silico modelling to generate predictions about them. Several limitations are therefore present regarding how far these results can be taken. The binding, safety and pharmacokinetic results are computational modelling results, generated using tools known for modelling pharmaceutical drug development but cannot be regarded with the same assurance as in vitro or in vivo biological results because there may be various other factors at play which could cause results to be significantly different. The molecular dynamics comprised three 20 ns runs per complex. Trajectories of this length can separate stable from unstable binding modes but cannot resolve fine differences in affinity, and a 20 ns window samples only a small fraction of the conformational space a ligand explores in vivo. The ADMET and pharmacokinetic values are model predictions rather than measurements: SwissADME and admetSAR 2.0 are trained largely on orally administered small molecules, and their estimates of blood-brain-barrier penetration and clearance carry substantial and largely uncharacterised error when extrapolated to an intranasal route. The PK-Sim profiles inherit that uncertainty, since the absorption parameters were themselves predicted rather than fitted to measured plasma or brain concentrations. Encapsulation efficiency, drug loading and release kinetics were not measured, so the characterisation data describe the particles themselves and say nothing about how much of either compound they carry or how it is released; until those values are determined the preparation cannot be described as a delivery system for these compounds. The study contains no biological validation of any kind. TrkB activation, signalling, and tau-aggregation inhibition remain to be demonstrated in cellular and animal systems.

These limitations highlight important future steps. Future work should be aimed to quantify nanoparticle encapsulation, loading and release; and to confirm 7,8-Dihydroxyflavone-driven TrkB phosphorylation and downstream signalling in SH-SY5Y cells and hippocampal neurons. Success through these stages would further justify nose-to-brain pharmacokinetics and efficacy.

Beyond molecular targets, this approach addresses a practical barrier to disease-modifying AD treatment. A self-administered intranasal small-molecule particle would overcome the infusion, imaging and monitoring limitations that current anti-amyloid antibodies require [6, 7] and would be expected to cost substantially less to produce than antibody therapies, although a thorough cost analysis was not carried out in this study. These advantages matter most where dementia’s burden is heaviest, in lower-income and rural populations across the globe.

This work combines two AD target matched compounds, a delivery route suited to brain exposure, as well as a preparable formulation into a testable therapeutic hypothesis. The computational and

physicochemical evidence presented are sufficient to justify biological validation, but supporting the claim of therapeutic effect requires further in vitro and in vivo testing.

## Methods

# Molecular docking

Structures for the TrkB receptor (PDB 4ASZ), tau protein (PDB 6GX5) and GSK-3β (PDB 1Q4L) were obtained from the RCSB Protein Data Bank and prepared in UCSF ChimeraX (v1.6) [24] by removing crystallographic solvent and adding hydrogen molecules. This was exported in PDB format. Three-dimensional conformers for 7,8-Dihydroxyflavone (PubChem CID 1880), EF24 (CID 66571561), donepezil (CID 3152) and memantine (CID 4054) were downloaded from PubChem, hydrogen molecules were added in UCSF ChimeraX and the result was exported in a Mol2 format. Static docking was run on SwissDock [19] using AutoDock Vina [20] with default parameters sampling the full protein surface. All twelve of the protein-ligand pairs were docked three times; reported ΔG are mean values. Docked complexes were inspected through UCSF ChimeraX to evaluate feasibility.

## Molecular dynamics simulation

The twelve docked complexes were prepared in CHARMM-GUI Solution Builder [25], solvated in rectangular TIP3P water boxes with 10 Å padding and 0.15 M KCl, and defined with the CHARMM36m force field. Simulations ran in GROMACS (v2022) [26] with GPU acceleration: energy minimisation, NVT equilibration at 300 K for 100 ps, NPT equilibration at 1 bar for 100 ps, and a 20 ns production run. Protein backbone and ligand RMSD were recorded with ‘gmx rms’ and mean hydrogen-bond counts with ‘gmx hbond’ over the simulation. Each pair was simulated three times.

# ADME and toxicity prediction

Ligand SMILES codes were obtained from PubChem. Blood-brain-barrier permeability, consensus LogP, aqueous solubility and drug-likeness were predicted using SwissADME [21]; Ames mutagenicity, rat oral LD50, and an overall toxicity screening with admetSAR 2.0 [22]. Each compound was submitted three times to each tool to ensure accuracy.

# Pharmacokinetic simulation

Oral and intranasal administration was simulated using PK-Sim (Open Systems Pharmacology Suite v11) with SwissADME-derived parameters. 7,8-Dihydroxyflavone was assigned a molecular weight of 254.24 g $mol^{-1}$, plasma protein binding of 80% and a 0.5 h half-life estimated from flavonoid literature; EF24 was assigned plasma protein binding of 90% and a 0.8 h half-life. A 100-individual virtual adult population was generated using age and sex distributions approximating Statistics Canada 2021 census data. Both

routes were simulated at a 50 mg dose over 24 h. Cmax, Tmax and 24 hour brain AUC were recorded from the output, with three runs per compound route combination.

# PLGA nanoparticle synthesis

Nanoparticles containing both 7,8-Dihydroxyflavone and EF24 were synthesized through an oil-in-water emulsion–solvent evaporation method across three independent batches. For each batch, polyvinyl alcohol (PVA; Sigma-Aldrich 363138) was dissolved in Milli-Q water (10 mL; 1.0% w/v) at roughly 80–90°C and filtered through 0.22 µm. Next, PLGA (10 mg; Sigma-Aldrich) was dissolved in dichloromethane (0.2 mL) by vortexing the solution at 2,500 RPM for 3 minutes, and 7,8-Dihydroxyflavone (0.3 mg) (CAS: 38183-03-8) and EF24 (0.3 mg) (CAS: 342808-40-6) added and dissolved in the solution. The organic phase was added dropwise to the PVA phase under magnetic stirring at 900 rpm in a fume hood with directed airflow for 30–45 min to evaporate solvent and form nanoparticles (Nanoparticle formation during oil-in-water emulsion–solvent evaporation is provided in Figure S2). The suspension was centrifuged at 1.5 RCF for 1.5 minutes, and the nanoparticle pellet was resuspended in 3 mL isotonic saline (pH 6.5).

# Nanoparticle characterisation

Nanoparticle size and polydispersity were measured through dynamic light scattering on a Malvern Zetasizer Nano ZS (Malvern Panalytical, Zetasizer Software v7.13). Each batch was diluted 1:100 in 0.22 µm-filtered Milli-Q water to filter out nanoparticles larger than 220 nm. The diluted suspension was then passed through a fresh 0.22 µm syringe filter before loading into the DLS cuvette (material refractive index 1.47, dispersant water, 25°C, 173° backscatter). Z-average diameter and PDI (cumulant fit) were recorded for each batch. Zeta potential was measured by electrophoretic light scattering on a separate aliquot diluted 1:50 in isotonic saline (pH 6.5). Data was processed in Zetasizer Software v7.13 and are reported as mean ± standard deviation across three independently prepared batches.

# Statistics and reproducibility

Docking ΔG values are reported as the mean of three docking runs per protein-ligand pair; ADMET predictions as the result of three independent submissions per compound. Molecular dynamics comprised three 20 ns simulations per complex. Nanoparticle measurements are reported as mean ± standard deviation across three independently synthesised batches. No inferential statistical tests were applied, as the study reports predicted and descriptive quantities rather than group comparisons.

## Declarations

# Competing interests

The authors declare no competing interests.

# Funding

This research received no external funding.

# Author Contribution

R.R. and V.K. designed the study, performed all computational analyses, carried out the nanoparticle synthesis and characterisation, and wrote the manuscript. B.W. supervised and aided in nanoparticle synthesis and characterisation. R.R. and V.K. contributed equally to this work. All authors reviewed and approved the final manuscript.

# Ethics Declaration

This study did not involve human participants, human data, or animal subjects. All experiments were computational (molecular docking, molecular dynamics, ADMET prediction, and pharmacokinetic simulation) or performed on synthesized chemical materials (PLGA nanoparticle formulation and physicochemical characterisation). No ethical approval or consent was therefore required.

# Data availability

The datasets generated and analysed during the current study are available in the Zenodo repository, https://doi.org/10.5281/zenodo.22240487. The macromolecular structure data analysed in this study are available in the Worldwide Protein Data Bank (wwPDB) under accession codes 4ASZ (TrkB), 6GX5 (tau) and 1Q4L (GSK-3β). Chemical structure data are available in PubChem under CIDs 1880, 66571561, 3152 and 4054.

## References

1. Alzheimer's Disease International. Dementia statistics. (2020). https://www.alzint.org/about/dementia-facts-figures/dementia-statistics/
2. World Health Organization. The top 10 causes of death. *WHO Fact. Sheets* (2024). https://www.who.int/news-room/fact-sheets/detail/the-top-10-causes-of-death
3. Dou, K. X. et al. Comparative safety and effectiveness of cholinesterase inhibitors and memantine for Alzheimer's disease: a network meta-analysis of 41 randomized controlled trials. *Alzheimers Res. Ther.* **10**, 126 (2018).

4. Yiannopoulou, K. G. & Papageorgiou, S. G. Current and future treatments in Alzheimer disease: an update. *J. Cent. Nerv. Syst. Dis.* **12**, 1179573520907397 (2020).
5. van Dyck, C. H. et al. Lecanemab in early Alzheimer's disease. *N Engl. J. Med.* **388**, 9–21 (2023).
6. Sims, J. R. et al. Donanemab in early symptomatic Alzheimer disease: the TRAILBLAZER-ALZ 2 randomized clinical trial. *JAMA* **330**, 512–527 (2023).
7. Honig, L. S. et al. Updated safety results from phase 3 lecanemab study in early Alzheimer's disease. *Alzheimers Res. Ther.* **16**, 105 (2024).
8. Congdon, E. E. et al. Tau-targeting therapies for Alzheimer disease: current status and future directions. *Nat. Rev. Neurol.* **19**, 715–736 (2023).
9. Minichiello, L. TrkB signalling pathways in LTP and learning. *Nat. Rev. Neurosci.* **10**, 850–860 (2009).
10. Rosa, E. & Fahnestock, M. CREB expression mediates amyloid β-induced basal BDNF downregulation. *Neurobiol. Aging*. **36**, 2406–2413 (2015).
11. Medeiros, R., Baglietto-Vargas, D. & LaFerla, F. M. The role of tau in Alzheimer's disease and related disorders. *CNS Neurosci. Ther.* **17**, 514–524 (2010).
12. Amidfar, M., de Oliveira, J., Kucharska, E., Budni, J. & Kim, Y. K. The role of CREB and BDNF in neurobiology and treatment of Alzheimer's disease. *Life Sci.* **257**, 118020 (2020).
13. Bathina, S. & Das, U. N. Brain-derived neurotrophic factor and its clinical implications. *Arch. Med. Sci.* **11**, 1164–1178 (2015).
14. Abbott, N. J. Blood–brain barrier structure and function and the challenges for CNS drug delivery. *J. Inherit. Metab. Dis.* **36**, 437–449 (2013).
15. Craparo, E. F. et al. mPEG-PLGA nanoparticles labelled with loaded or conjugated Rhodamine-B for potential nose-to-brain delivery. *Pharmaceutics* **13**, 1508 (2021).
16. Jang, S. W. et al. A selective TrkB agonist with potent neurotrophic activities by 7,8-dihydroxyflavone. *Proc. Natl Acad. Sci. USA* 107, 2687–2692 (2010).
17. Numakawa, T. & Odaka, H. Brain-derived neurotrophic factor signaling in the pathophysiology of Alzheimer's disease: beneficial effects of flavonoids for neuroprotection. *Int. J. Mol. Sci.* **22**, 5719 (2021).
18. Hsiao, P. C. et al. The curcumin analogue EF-24 triggers p38 MAPK-mediated apoptotic cell death via inducing PP2A-modulated ERK deactivation in human acute myeloid leukemia cells. *Cancers* **12**, 2163 (2020).
19. Grosdidier, A., Zoete, V. & Michielin, O. SwissDock, a protein–small molecule docking web service based on EADock DSS. *Nucleic Acids Res.* **39**, W270–W277 (2011).
20. Trott, O. & Olson, A. J. AutoDock Vina: improving the speed and accuracy of docking with a new scoring function, efficient optimization, and multithreading. *J. Comput. Chem.* **31**, 455–461 (2010).
21. Daina, A., Michielin, O. & Zoete, V. SwissADME: a free web tool to evaluate pharmacokinetics, drug-likeness and medicinal chemistry friendliness of small molecules. *Sci. Rep.* **7**, 42717 (2017).

22. Yang, H. et al. admetSAR 2.0: web-service for prediction and optimization of chemical ADMET properties. *Bioinformatics* **35**, 1067–1069 (2019).
23. Meng, X. Y., Zhang, H. X., Mezei, M. & Cui, M. Molecular docking: a powerful approach for structure-based drug discovery. *Curr. Comput. Aided Drug Des.* **7**, 146–157 (2011).
24. Pettersen, E. F. et al. UCSF ChimeraX: structure visualization for researchers, educators, and developers. *Protein Sci.* **30**, 70–82 (2021).
25. Jo, S., Kim, T., Iyer, V. G. & Im, W. CHARMM-GUI: a web-based graphical user interface for CHARMM. *J. Comput. Chem.* **29**, 1859–1865 (2008).
26. Abraham, M. J. et al. GROMACS: high performance molecular simulations through multi-level parallelism from laptops to supercomputers. *SoftwareX* **1–2**, 19–25 (2015).

# Figures

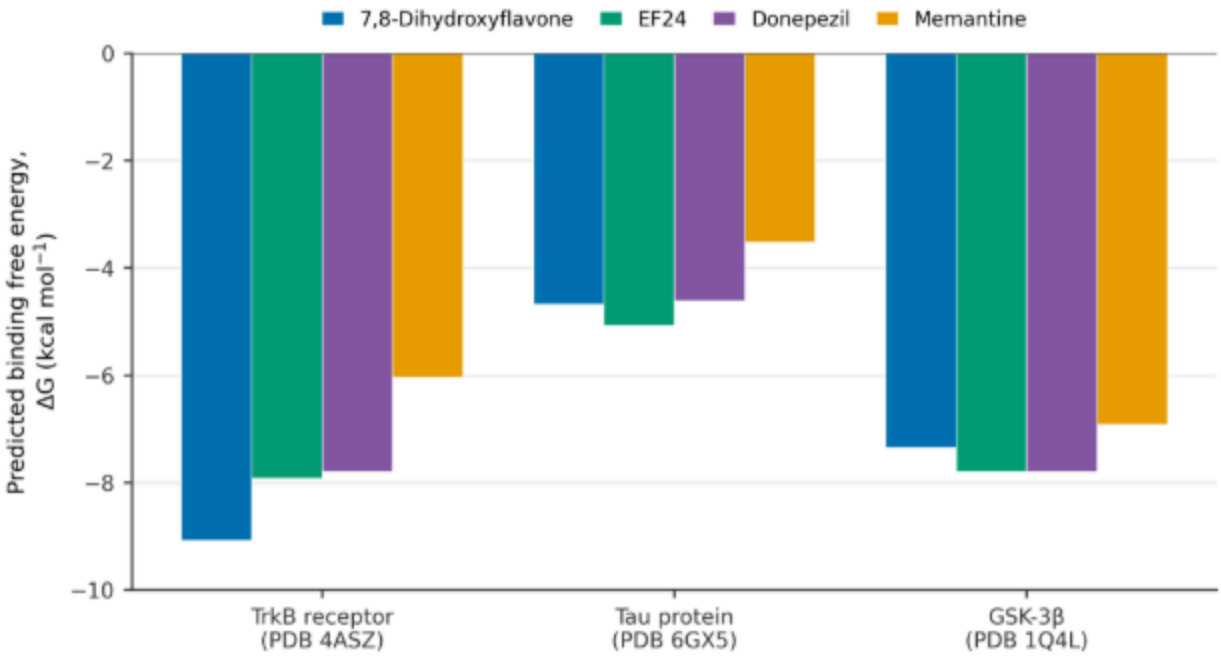



**Figure 1**

*Molecular docking binding energies for 7,8-Dihydroxyflavone, EF24, donepezil and memantine at three Alzheimer's disease-relevant protein targets.* Predicted free energy of binding (ΔG, kcal mol⁻¹) at the TrkB receptor (PDB 4ASZ), tau protein (PDB 6GX5) and GSK-3β (PDB 1Q4L); more negative values indicate stronger predicted binding. Structures were prepared in UCSF ChimeraX and docked in SwissDock with AutoDock Vina under default blind-docking parameters. Bars are the mean of three docking runs per compound–protein pair.

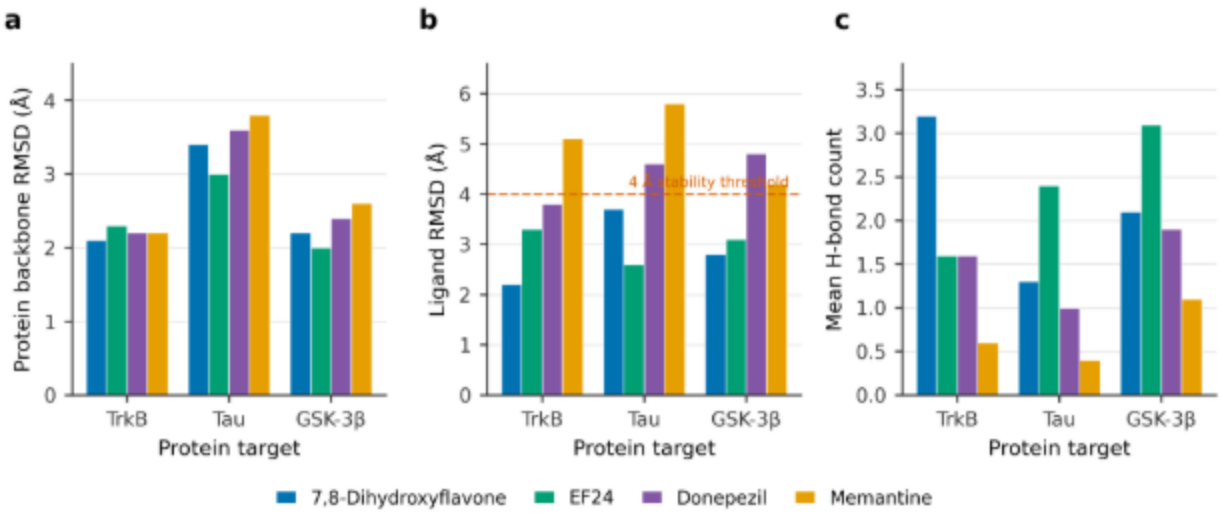



**Figure 2**

*Molecular dynamics stability metrics for all twelve protein–ligand pairs over a 20-nanosecond trajectory.* (a) Protein backbone RMSD (Å) for the TrkB receptor, tau protein and GSK-3β with each compound. (b) Ligand RMSD (Å); the dashed line at 4 Å marks the stability threshold. (c) Mean hydrogen-bond count over the trajectory. Systems were built in CHARMM-GUI with the CHARMM36m force field, TIP3P water and 0.15 M KCl and simulated in GROMACS. Each bar is the mean of three 20 ns runs.

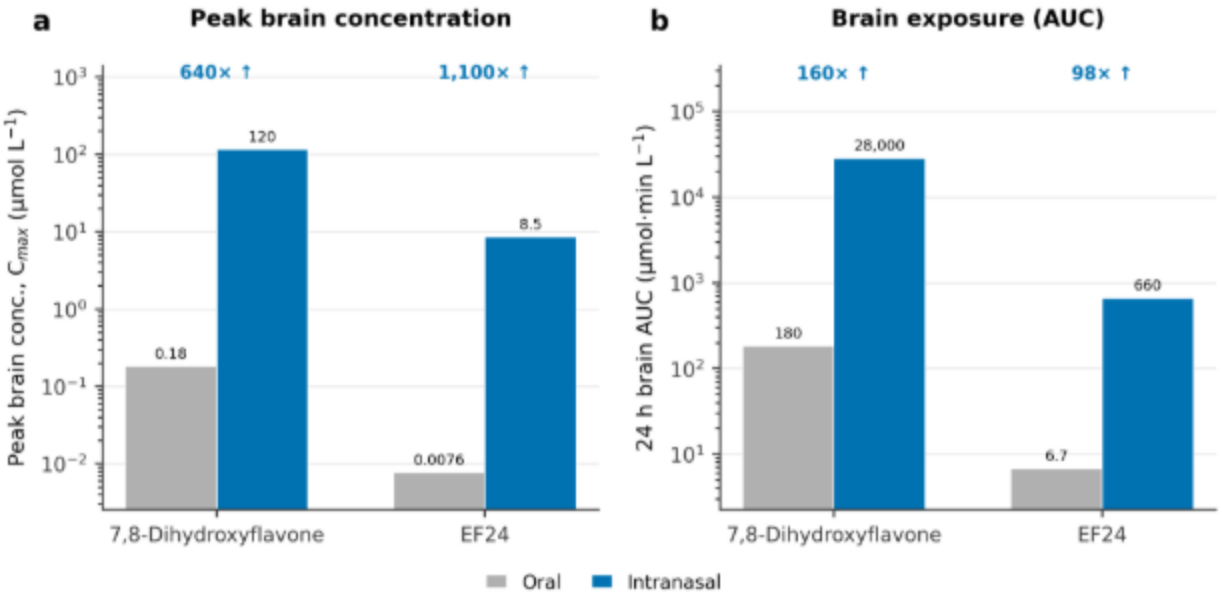



**Figure 3**

*Simulated brain pharmacokinetics for 7,8-Dihydroxyflavone and EF24 under oral and intranasal delivery over 24 hours.* (a) Peak brain concentration (Cmax, µmol L⁻¹) and (b) 24-hour brain AUC (µmol·min L⁻¹) on a logarithmic scale; blue arrows give the intranasal/oral fold ratio. Simulations were run in PK-Sim on a virtual adult population (n = 100) parameterised to Canadian demographics at a 50 mg dose. Bars are

the mean of three runs. Absolute magnitudes depend on estimated absorption and protein-binding parameters and should be read as illustrative.

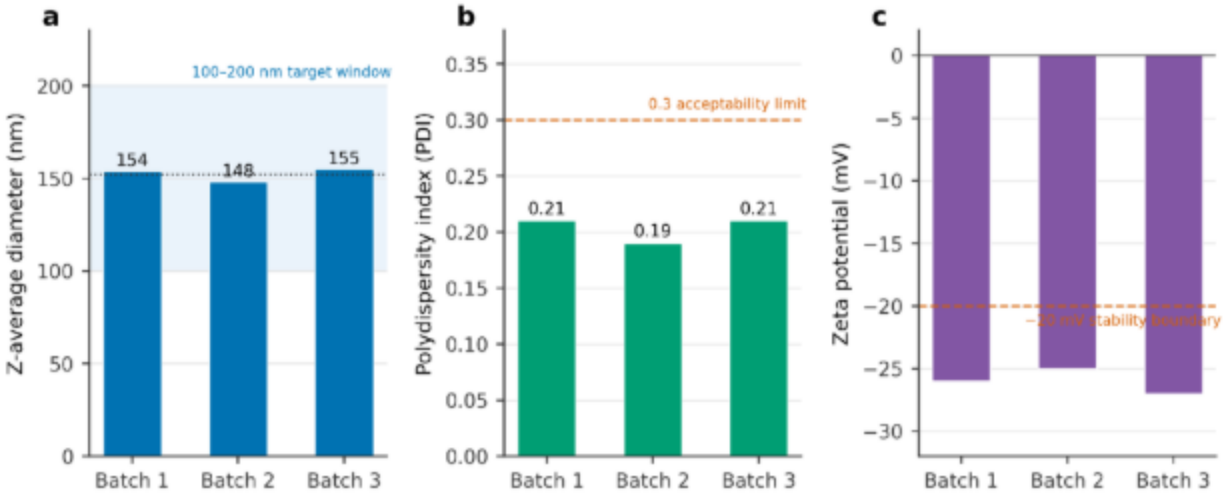



**Figure 4**

*Physical characterisation of PLGA nanoparticles co-loading 7,8-Dihydroxyflavone and EF24 across three independent batches.* (a) Z-average diameter (nm) by dynamic light scattering; shaded band, 100–200 nm target window; dotted line, batch mean. (b) Polydispersity index from cumulant fit; dashed line, 0.3 upper limit. (c) Zeta potential (mV) by electrophoretic light scattering; dashed line, −20 mV stability boundary. All measurements used a Malvern Zetasizer Nano ZS; bars are individual batch values.

## Supplementary Files

This is a list of supplementary files associated with this preprint. Click to download.

- NSRAlzheimersDiseaseSup.InfoB.W.docx